

Supplementary Information

Tandem electrocatalytic benzylic alcohols oxidation and aldol condensation for efficient valuable α,β -unsaturated ketones production

Yifan Yan,^{‡a} Xi Cai,^{‡a} Jiangrong Yang,^{‡a} Yu Fu,^a Qiwei Shi,^a Pengjie Hao,^a Hua Zhou,^a
Zhenhua Li,^{*a,c} Mingfei Shao,^{*a,c} Haohong Duan^{*b,d,e}

^aState Key Laboratory of Chemical Resource Engineering, College of Chemistry, Beijing
University of Chemical Technology, Beijing 100029, China

^bDepartment of Chemistry, Tsinghua University, Beijing 100084, China

^cInstitute for Innovation in Resource Chemical Engineering, Quzhou 324000, China

^dHaihe Laboratory of Sustainable Chemical Transformations, Tianjin 300192, China

^eEngineering Research Center of Advanced Rare Earth Materials, (Ministry of Education),
Department of Chemistry, Tsinghua University, Beijing, 100084, China

[‡]Yifan Yan, Xi Cai and Jiangrong Yang contributed equally to this work.

*Correspondence and requests for materials should be addressed to Z.L. (email:
LZH0307@mail.buct.edu.cn), M.S. (email: *shaomf@mail.buct.edu.cn*) and H.D. (email:
hhduan@mail.tsinghua.edu.cn).

Methods

Materials and reagents.

Except noted, all chemicals were purchased and used without further purification. Deionized water was used throughout the experiments. Copper nitrate ($\text{Cu}(\text{NO}_3)_2$), cobalt nitrate ($\text{Co}(\text{NO}_3)_2$), nickel nitrate ($\text{Ni}(\text{NO}_3)_2$), hydrochloric acid (HCl , 36.5–38 wt%) and sulfuric acid (H_2SO_4) were purchased from Sinopharm Chemical Reagent (Beijing Co., Ltd.). Benzyl alcohol ($\text{C}_7\text{H}_8\text{O}$, $\geq 99\%$), cetyl trimethyl ammonium bromide (CTAB, $\text{C}_{19}\text{H}_{42}\text{BrN}$) and acetone ($\text{C}_3\text{H}_6\text{O}$, $\geq 99\%$) was obtained from Shanghai Macklin Biochemical Co., Ltd.

Synthesis of CuO nanosheets.

Nickel foam (NF) was used as matrix for growing CuO nanosheets. Initially, NF ($25 \times 40 \times 1.5$ mm) was sequentially washed with dilute HCl (1 M), ethanol, and deionized water (each for 10 min) to remove surficial oxides and contaminants. Then, add $\text{Cu}(\text{NO}_3)_2 \cdot 3\text{H}_2\text{O}$ (2.0 mmol) and CTAB (0.25 g) into ethanol (30 mL) to obtain a mixed solution. Pour this mixed solution into the reaction vessel with nickel foam placed inside. Subsequently, react at 180°C for 24 hours to obtain $\text{Cu}(\text{OH})_2$ nanosheets. After thoroughly washing five times with ethanol and deionized water, vacuum dry at 70°C for 12 hours. Finally, place the $\text{Cu}(\text{OH})_2$ nanosheets in a muffle furnace and calcine at 350°C for 2 hours to obtain CuO nanosheets.

Synthesis of Au/CuO.

Au particles were electrodeposited on CuO in a three-electrode configuration using saturated calomel electrode (SCE) reference electrode, Pt foil as counter electrode, and NF supported CuO nanosheets as working electrode, respectively. The electrolyte was 0.1 M NaCl aqueous solution containing 5 mM HAuCl_4 . Specifically, Au NPs were deposited on CuO by stepping the potential to -0.6 V vs. SCE for 5 s, followed by stepping back to -0.2 V vs. SCE for 5 s for five cycles. The pure Au catalyst was prepared via the similar electrodeposition method by directly using Ni foam as the working electrode. Ni foam supported NiOOH, CoOOH were prepared based on previous reports¹ and Au particles were electrodeposited on them using the similar method of Au/CuO.

Characterizations.

X-ray diffraction patterns were collected on a Shimadzu XRD-6000 diffractometer using a Cu K α source, with a scan range of 10–55° and scan step of 5° min⁻¹. X-ray photoelectron spectra (XPS) were performed on a Thermo VG ESCALAB 250 X-ray photoelectron spectrometer at a pressure of about 2×10⁻⁹ Pa using Al K α X-rays as the excitation source. Scanning electron microscope (SEM) images were recorded by a Zeiss SUPRA 55 Field Emission SEM with an accelerating voltage of 20 kV. Transmission electron microscopy (TEM) images were recorded with JEOL JEM-2010 high resolution (HR-)TEM with an accelerating voltage of 200 kV. Metal contents in catalysts were determined by ICP-MS on a Thermo ICAP6300 Radial.

Electrochemical measurement.

All electrochemical measurements for benzyl alcohol oxidation were performed in 0.1 M KOH electrolyte at room temperature on an electrochemical workstation (CHI 760E, CH Instruments, Inc.). The electrochemical tests were performed in a three-electrode system in a membrane-free glass beaker, using Ag/AgCl electrode (with saturated KCl) and Pt foil as reference and counter electrode, respectively. Specially, the H-cell is utilized to couple anodic and cathodic reactions for the simultaneous preparation of high-value-added organic products. Linear scan voltammetry (LSV) curves of catalysts were acquired from -0.6 V to 0.7 V vs. Ag/AgCl at a scan rate of 10 mV s⁻¹. All of the electrocatalytic reactions were conducted at ambient pressure and temperature, unless otherwise specified. All potentials measured against Ag/AgCl were converted to the reversible hydrogen electrode (RHE) scale using the following equations:

$$E_{\text{RHE}} = E_{\text{Ag/AgCl}} + E_{\text{Ag/AgCl vs. NHE}} + 0.059 \text{ pH} \quad (1)$$

where $E_{\text{Ag/AgCl vs. NHE}}$ in eq (1) is 0.197 V at 20 °C.

The FEs of all the products were calculated based on their corresponding electron transfer per molecule oxidation using the following equations.

$$\text{Faradaic efficiency} = \frac{n_e \times n_{\text{products}} \times F}{Q} \times 100\% \quad (2)$$

where n_e is the number of electrons required to oxidize benzyl alcohol to products. n_{products}

is the productivity of products, F is Faraday constant ($F = 96485$), Q is the quantity of electric charge.

The selectivity of the products was calculated based on total moles of benzyl alcohol oxidation products using the following equations.

$$\text{Selectivity} = \frac{n_{\text{product}}}{n_{\text{converted benzyl alcohol}}} \times 100\% \quad (3)$$

The liquid products were quantified by high performance liquid chromatography (HPLC; Angilent 1200 Infinity Series) equipped with C18 column (Cosmosil C18-MS-II) using MeCN/H₂O/H₃PO₄ (40/60/0.05) as mobile phase and detected by UV detector at 220 nm. Some products in Figure 2g were analyzed by gas chromatography mass spectrometry (GC-MS, Agilent Technologies, GC7890B, MS 5977B).

Supplementary figures

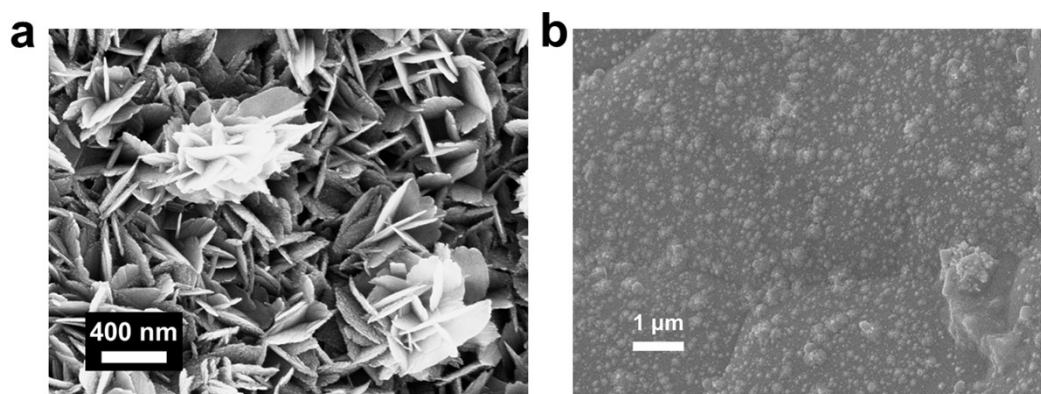


Figure S1. SEM images of (a) CuO, (b) Au on Ni foam.

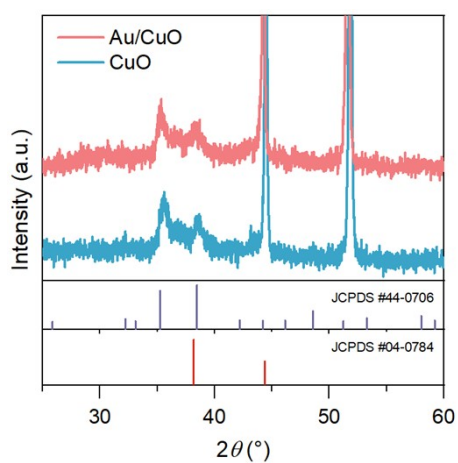


Figure S2. XRD patterns of Au/CuO and CuO catalysts.

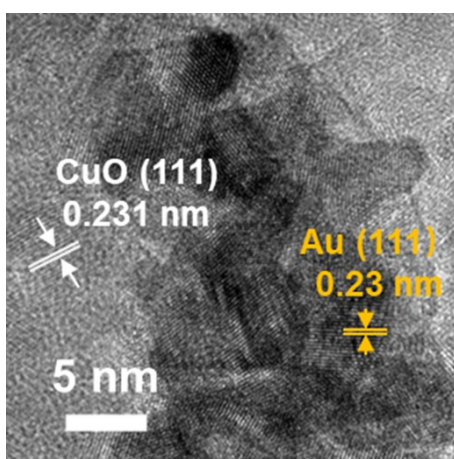


Figure S3. HRTEM image of Au/CuO.

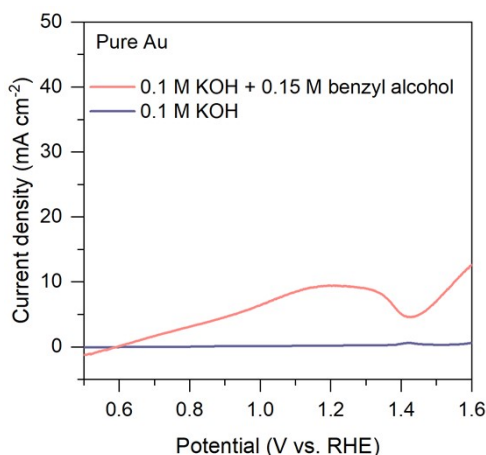


Figure S4. LSV curves of pure Au on Ni foam in 0.1 M KOH and 0.1 M KOH with 0.15 M benzyl alcohol at scan rate of 10 mV s^{-1} .

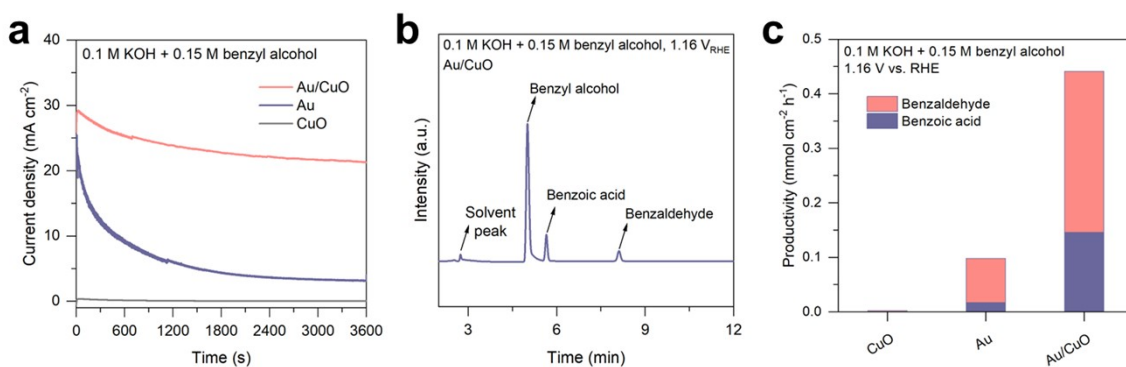


Figure S5. (a) $I-t$ curves of different catalysts in 0.1 M KOH with 0.15 M benzyl alcohol at 1.16 V vs. RHE. (b) HPLC chromatogram of benzyl alcohol electrooxidation products over Au/CuO in 1 hour. (c) All benzyl alcohol electrooxidation products over different catalysts at 1.16 V vs. RHE.

As shown in the Figure S5a, the Au/CuO cooperative catalyst exhibits a much higher current density than pure Au, indicating a higher electron transfer rate within the same time frame. This suggests that benzyl alcohol is more readily overoxidized on Au/CuO. As a result, the selectivity toward benzaldehyde on Au/CuO is lower compared to that on pure Au.

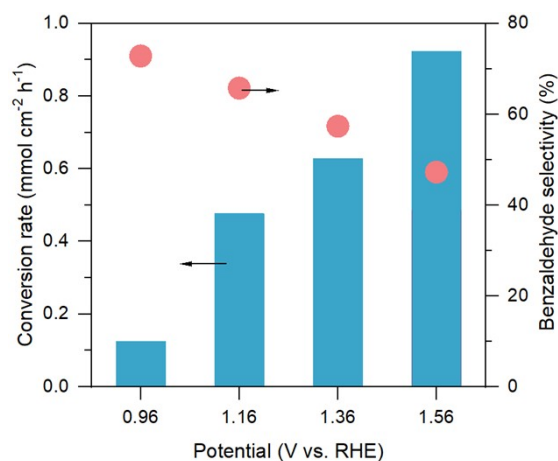


Figure S6. Conversion rate of benzyl alcohol oxidation and the corresponding selectivity of benzaldehyde at different potentials over Au/CuO.

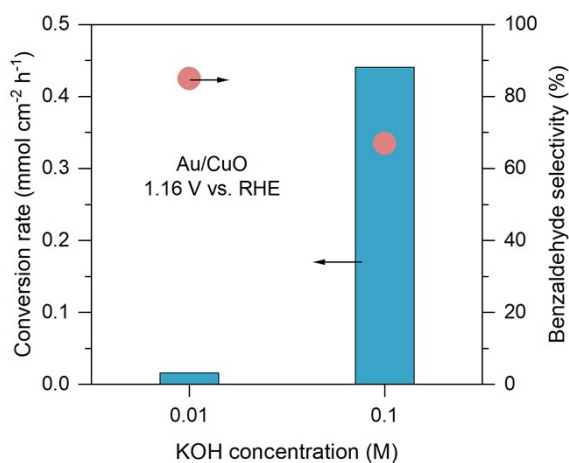


Figure S7. Conversion rate of benzyl alcohol and benzaldehyde selectivity under different KOH concentration with 0.15 M benzyl alcohol in 1 hour.

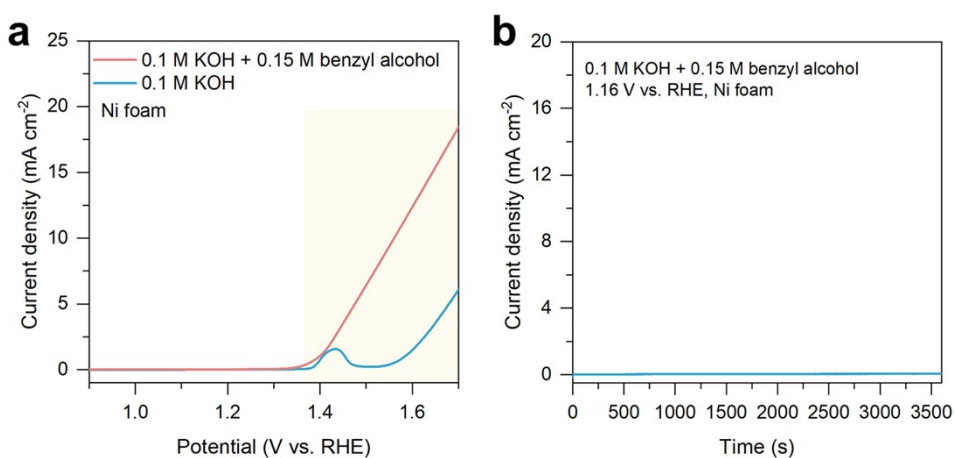


Figure S8. (a) LSV curves of Ni foam at scan rate of 10 mV s⁻¹ in 3 M KOH with 0.3 M EG. (b) I-t curves of Ni foam at 1.25 V vs. RHE in 3 M KOH with 0.3 M EG.

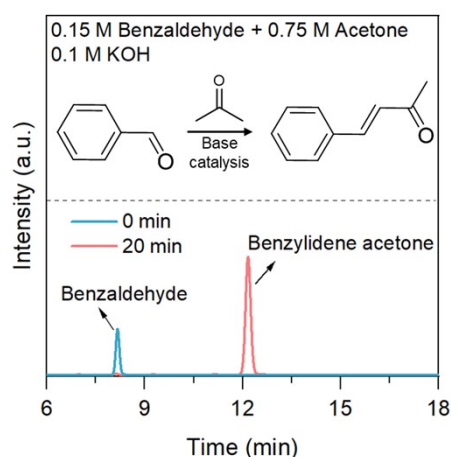


Figure S9. HPLC chromatogram of 0.15 M benzaldehyde and 0.75 M acetone in 0.1 M KOH before (0 min) and after 20 min of spontaneous reaction.

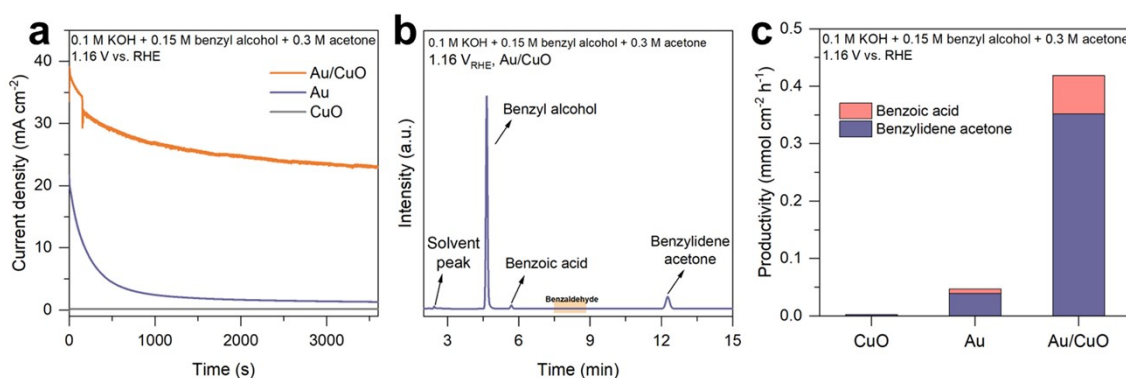


Figure S10. (a) *I-t* curves of different samples in 0.1 M KOH with 0.15 M benzyl alcohol and 0.3 M acetone at 1.16 V vs. RHE. (b) HPLC chromatogram of benzyl alcohol electrooxidation products (with acetone) over Au/CuO in 1 hour. (c) All benzyl alcohol electrooxidation products (with acetone) over different catalysts at 1.16 V vs. RHE.

In our system, the aldol condensation between in-situ generated benzaldehyde and acetone proceeds rapidly in alkaline solution, as evidenced by the complete conversion of 0.15 M (15 mmol) benzaldehyde to benzylidene acetone within 20 minutes (Figure S9), which is significantly faster than the electrooxidation rate of benzyl alcohol ($0.44 \text{ mmol cm}^{-2} \text{ h}^{-1}$ at 1.16 V). This indicates that the aldol condensation step is not rate-limiting under our reaction conditions. Additionally, we observed that the presence of acetone significantly enhances the selectivity of Au/CuO, with the selectivity toward benzylidene acetone reaching 84% in the presence of acetone, compared to only 67% selectivity toward benzaldehyde without acetone. This improvement is attributed to the rapid condensation of benzaldehyde with acetone,

lowering the amount of benzaldehyde being oxidized to benzoic acid. This indicates that the overall reaction rate is governed by the interfacial electrochemical oxidation step. Taken together, these findings suggest that the overall tandem reaction is governed by the interfacial electrochemical oxidation of benzyl alcohol, rather than the aldol condensation step.

In our future work, we will focus on designing more efficient catalysts and further optimizing the reaction conditions to achieve high current density while maintaining high selectivity toward aldehydes.

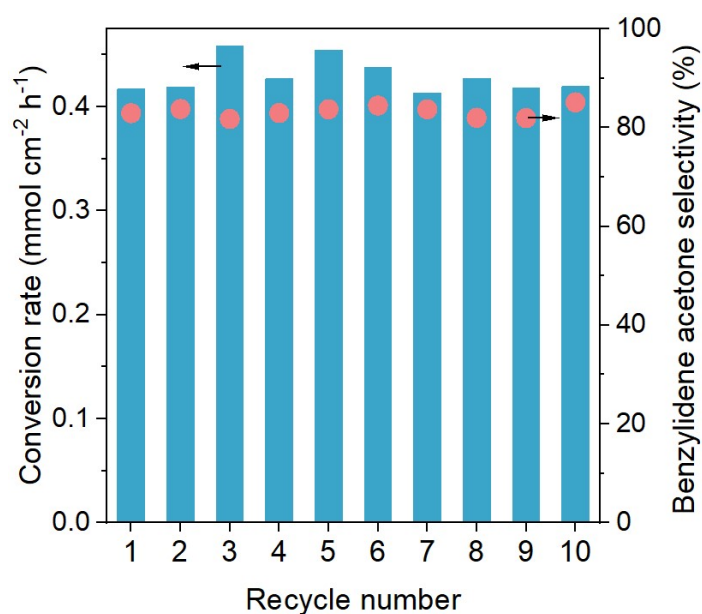


Figure S11. Stability test (10 batches, 10 h).

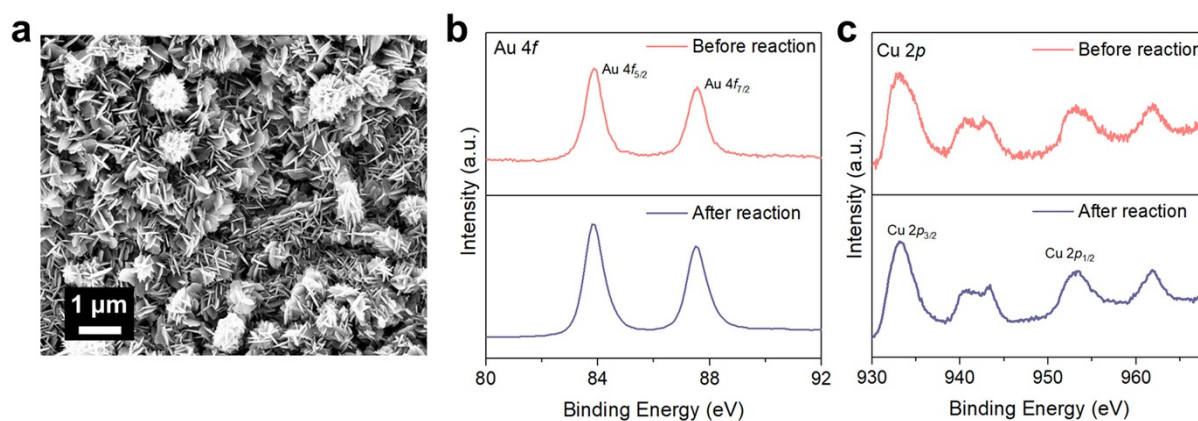


Figure S12. (a) SEM images of Au/CuO after 10 cycles reaction. (b) High-resolution Au 4*f* XPS spectra. (c) High-resolution Cu 2*p* XPS spectra.

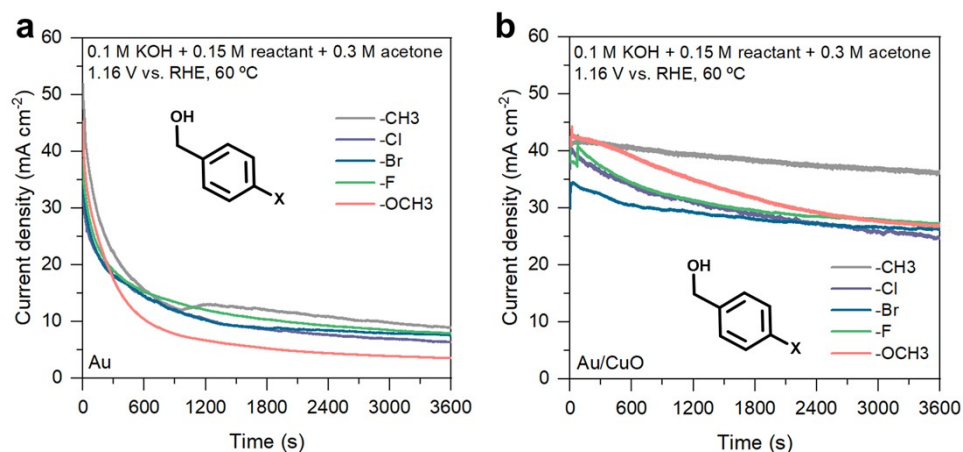


Figure S13. Current-time ($I-t$) curves of (a) Au and (b) Au/CuO in 0.1 M KOH with 0.15 M benzyl alcohols with different substituents ($-Cl$, $-F$, $-Br$, $-CH_3$, $-OCH_3$) and 0.3 M acetone at 60 °C at 1.16 V vs. RHE.

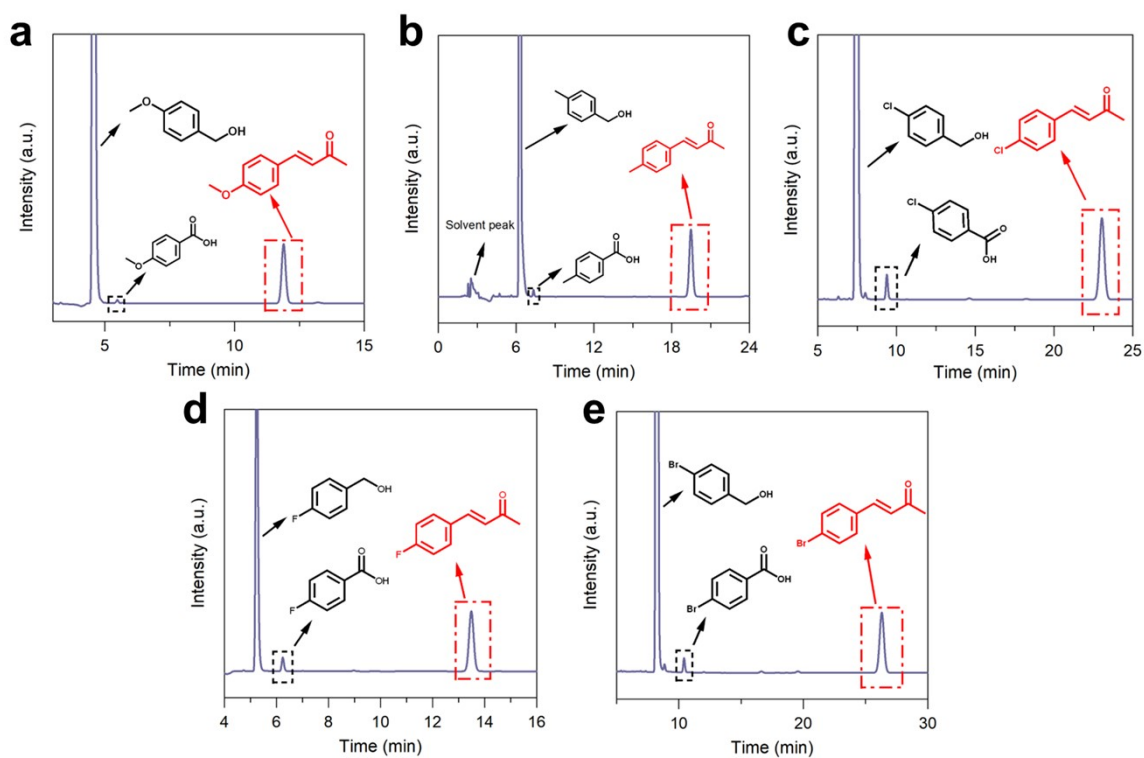


Figure S14. HPLC chromatogram of electrooxidation products over Au/CuO in 0.1 M KOH with 0.15 M benzyl alcohols with different substituents ($-Cl$, $-F$, $-Br$, $-CH_3$, $-OCH_3$) and 0.3 M acetone at 60 °C at 1.16 V vs. RHE in 1 hour.

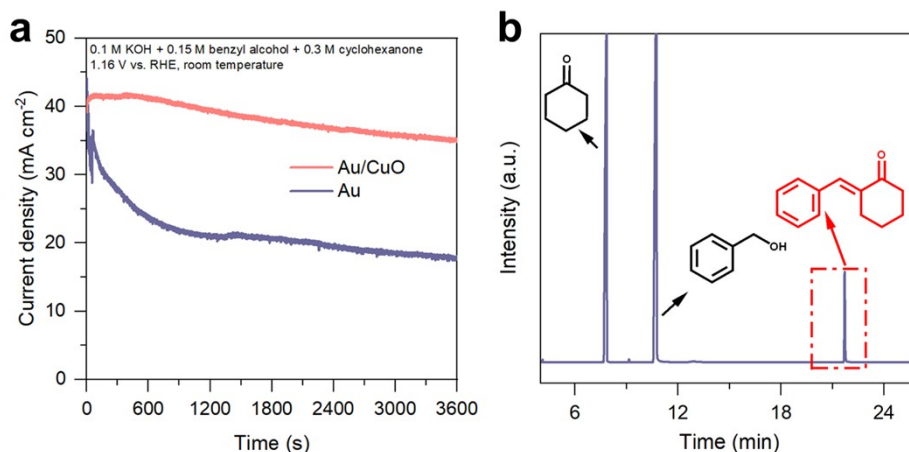


Figure S15. (a) Current-time ($I-t$) curves of different catalysts in 0.1 M KOH with 0.15 M benzyl alcohol and 0.3 M cyclohexanone at 1.16 V vs. RHE. (b) Gas chromatogram of electrooxidation products over Au/CuO in 1 hour.

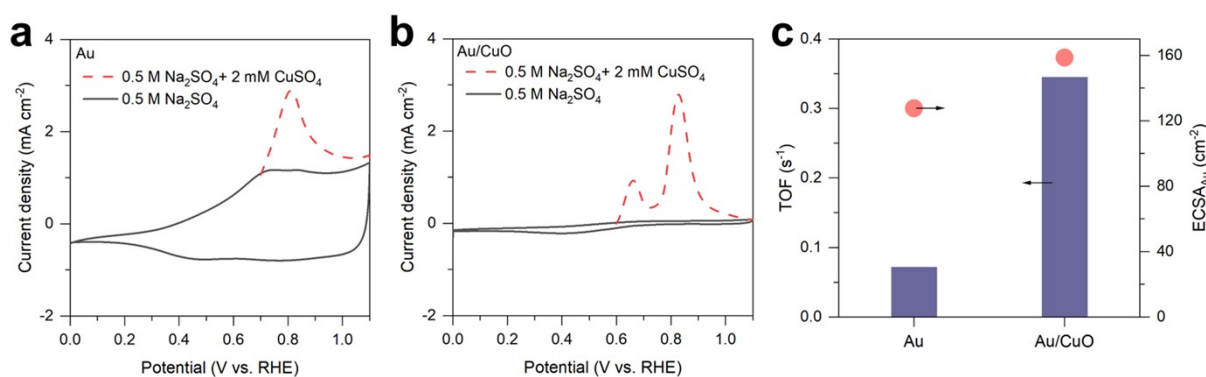


Figure S16. Underpotential deposition of Cu for measuring the ECSA of Au over (a) pure Au and (b) Au/CuO catalysts. Scan rate: 5 mV s^{-1} . (c) TOF values of benzyl alcohol oxidation over Au/CuO and Au at 1.16 V vs RHE.²

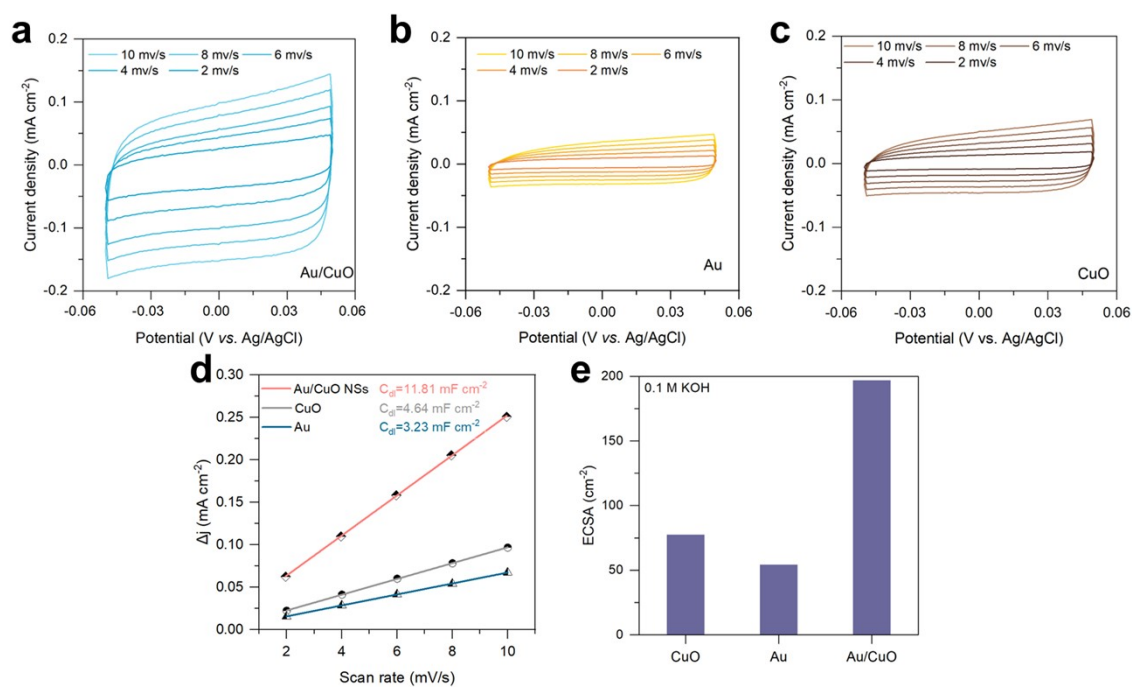


Figure S17. CV curves of (a) Au/CuO, (b) Au and (c) CuO measured in a non-Faradaic region of the voltammogram at the following scan rate: 2, 4, 6, 8, and 10 mV/s.³ (d) Au, CuO and Au/CuO current density–scanning rate plots. (e) Total ECSA of different samples.^{4,5}

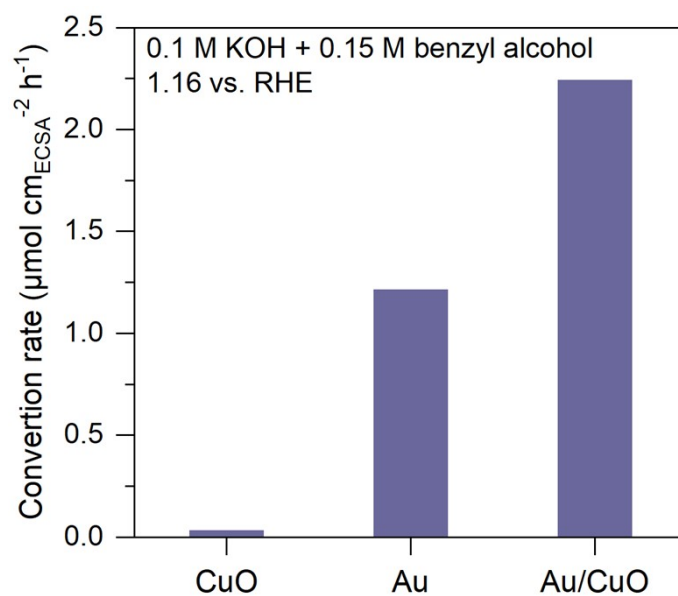


Figure S18. Conversion rate of benzyl alcohol over different samples after normalizing by total ECSA.

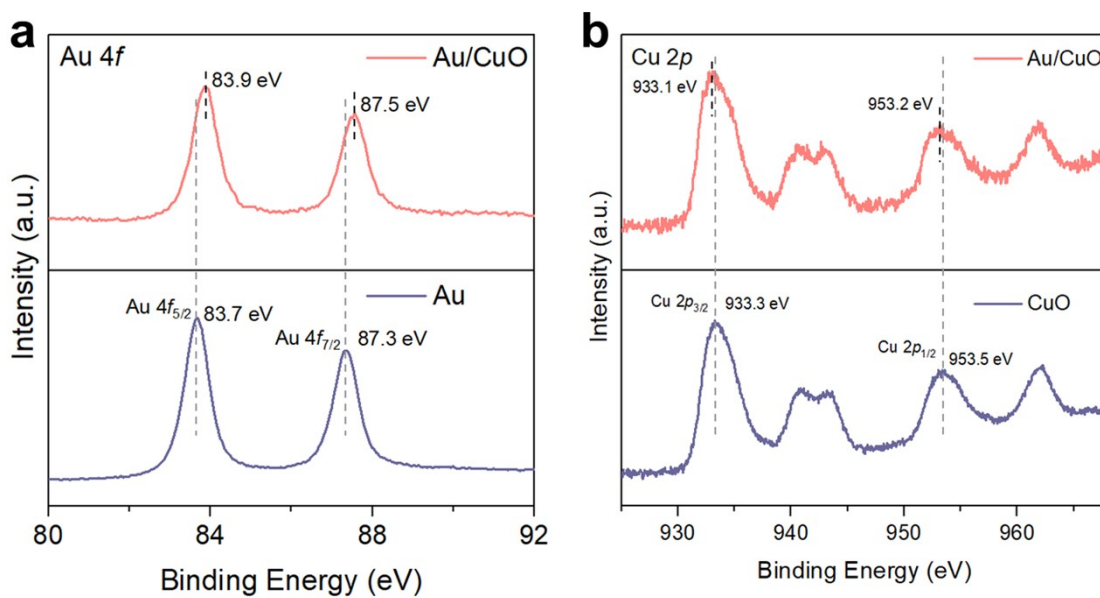


Figure S19. (a) High-resolution Au 4f XPS spectra. (b) High-resolution Cu 2p XPS spectra of Au and Au/CuO.

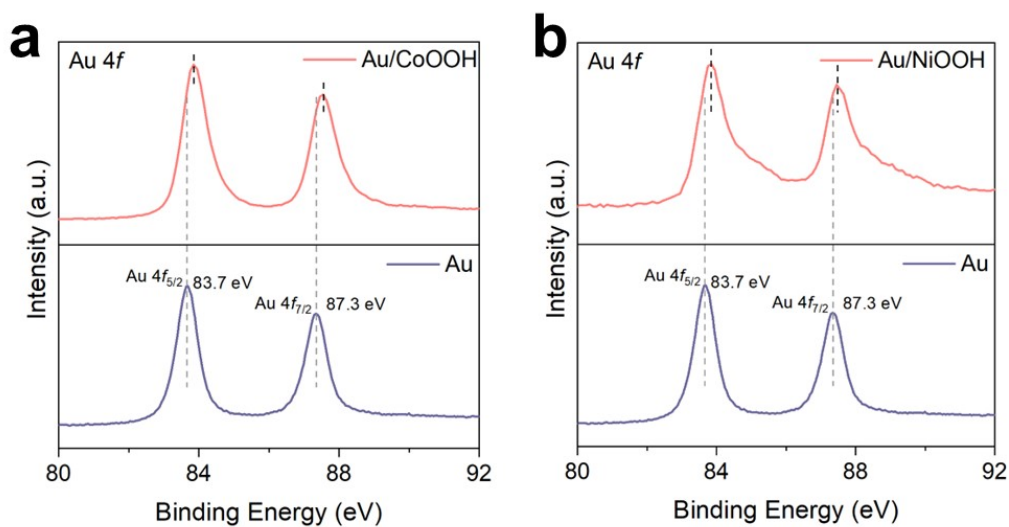


Figure S20. High-resolution Au 4f XPS spectra of Au, Au/CoOOH and Au/NiOOH.

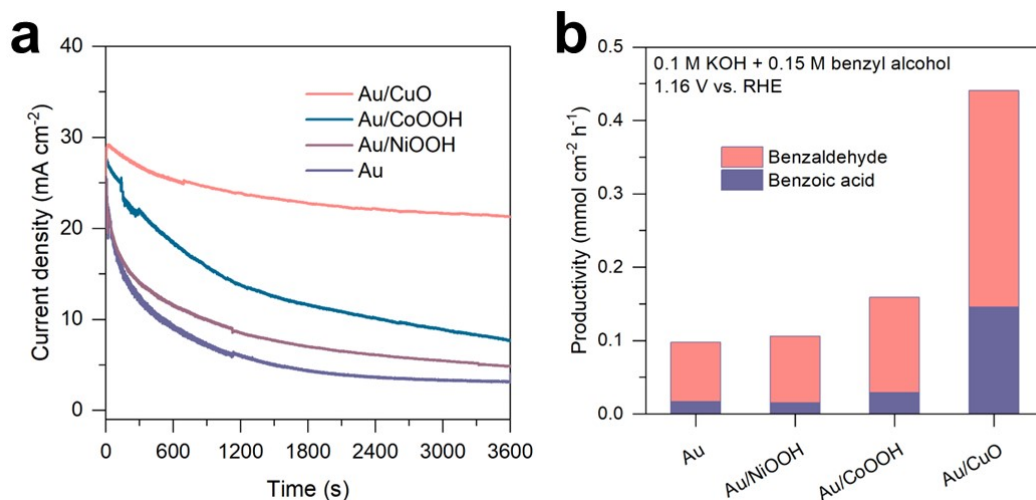


Figure S21. (a) *I-t* curves of different catalysts in 0.1 M KOH with 0.15 M benzyl alcohol at 1.16 V vs. RHE. (c) Benzyl alcohol electrooxidation products over different catalysts at 1.16 V vs. RHE.

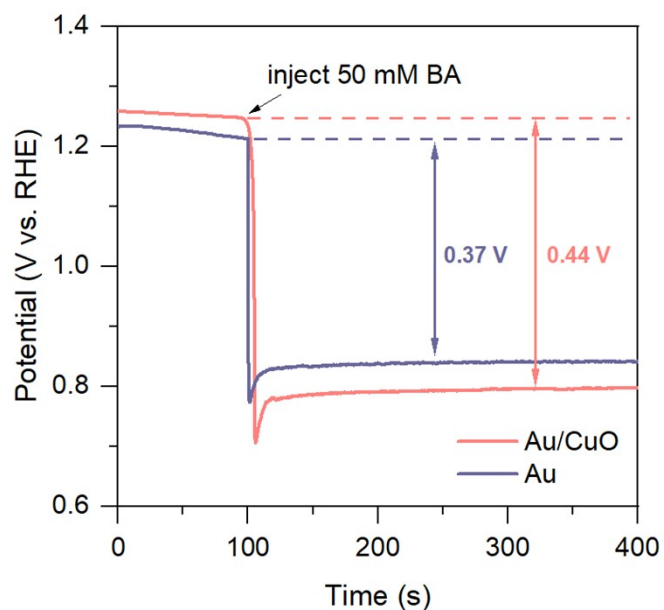


Figure S22. The OCP of the Au/CuO and Au samples in 0.1 M KOH solution before and after benzyl alcohol (BA) injected.

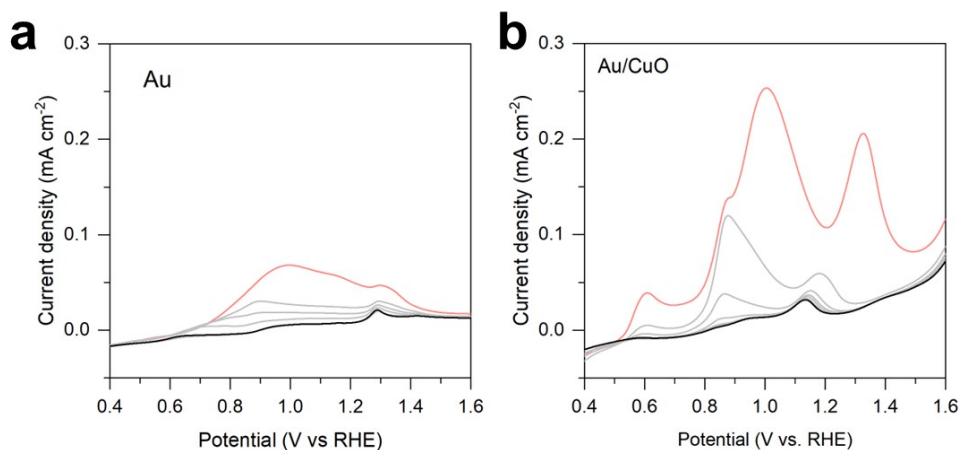


Figure S23. Adsorbate stripping from benzyl alcohol adsorption on (a) Au and (b) Au/CuO catalysts. Reaction conditions: 0.1 M KOH; scan rate = 10 mV s⁻¹. First scan (red line) and subsequent scans.

For the electrochemical adsorbate-stripping measurements, Au/CuO and Au samples (on glassy carbon electrodes) were initially submerged in a 0.1 M KOH solution with 0.15 M benzyl alcohol and maintained at 0.2 V vs. RHE for 1 minute to ensure adsorption of benzyl alcohol. The potential of 0.2 V vs. RHE was selected as it is sufficiently high to facilitate benzyl alcohol adsorption while preventing its oxidation. Subsequently, the electrodes were rinsed in O₂-free ultrapure water to eliminate excess benzyl alcohol and then transferred to an electrochemical cell containing 0.1 M KOH, where the adsorbed benzyl alcohol was electrocatalytically stripped via LSV scan. The quantity of adsorbed benzyl alcohol over catalysts was determined by calculating the oxidation charges ($Q_{\text{Ox(BA)}}$) from the benzyl alcohol oxidation peaks.⁶

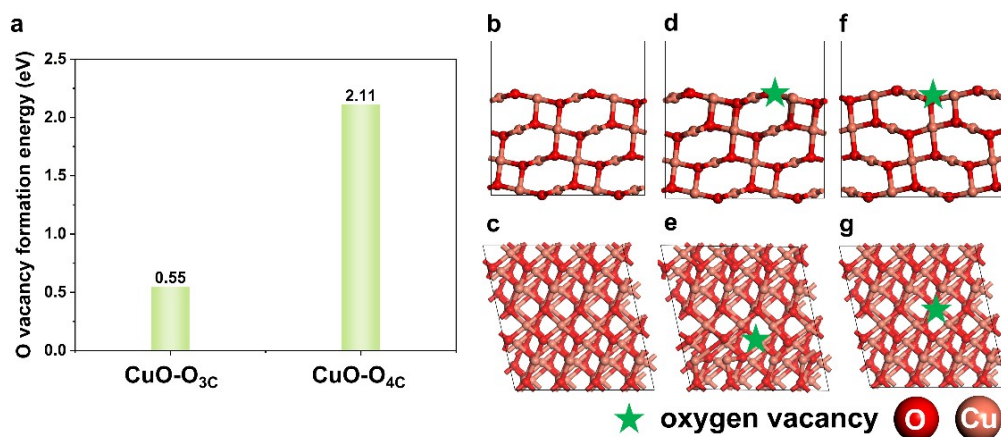


Figure S24. (a) The formation energies of oxygen vacancy with different coordinate numbers. The side view and the top view of the model of the CuO-P surface (b and c), the CuO-O_{3C} surface (d and e), and the CuO-O_{4C} surface (f and g), respectively. The color for each element is labeled.

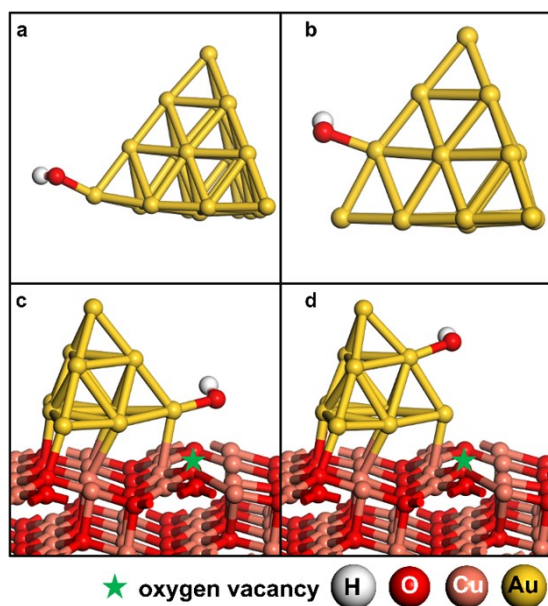


Figure S25. The model of OH* on the vertex site and the edge site on Au (a and b) and Au/CuO (c and d), respectively. The color for each element is labeled.

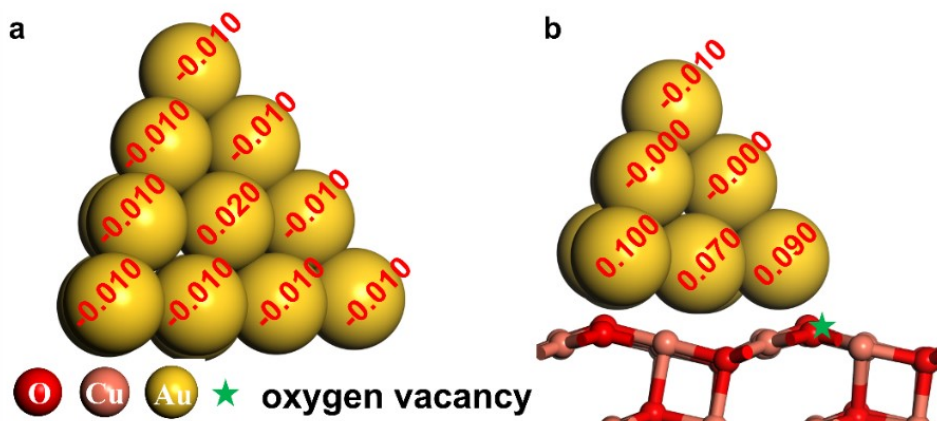


Figure S26. Hirshfeld charge analysis of Au atoms in modules Au (a) and Au/CuO (b). The color for each element is labeled.

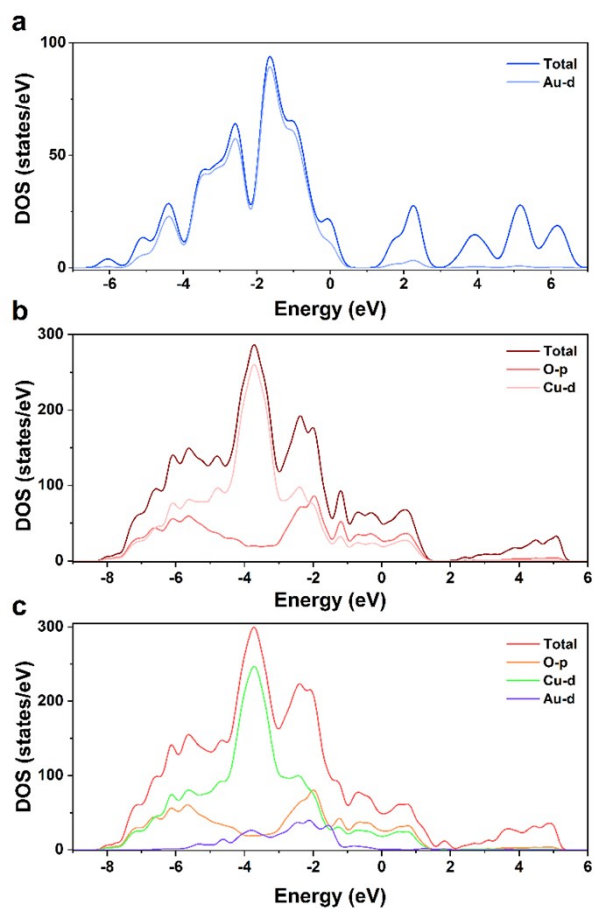


Figure S27. The total density of states (TDOS) and partial of states (PDOS) projected on the $5d$ orbits of Au atoms for Au (a), $2p$ orbits of O atoms and $3d$ orbits of Cu atoms for CuO (b), and $2p$ orbits of O atoms, $3d$ orbits of Cu atoms and $5d$ orbits of Au atoms for Au/CuO (c), respectively.

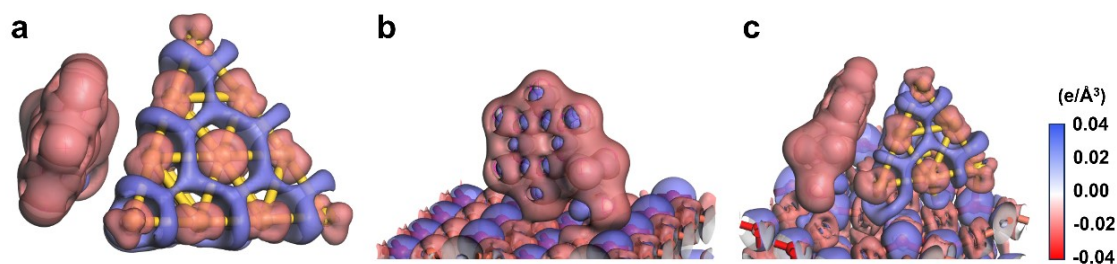


Figure S28. The charge density difference plots for benzyl alcohol adsorbed on Au (a), CuO (b) and Au/CuO (c), respectively. The red (blue) distribution corresponds to the charge accumulation (depletion).

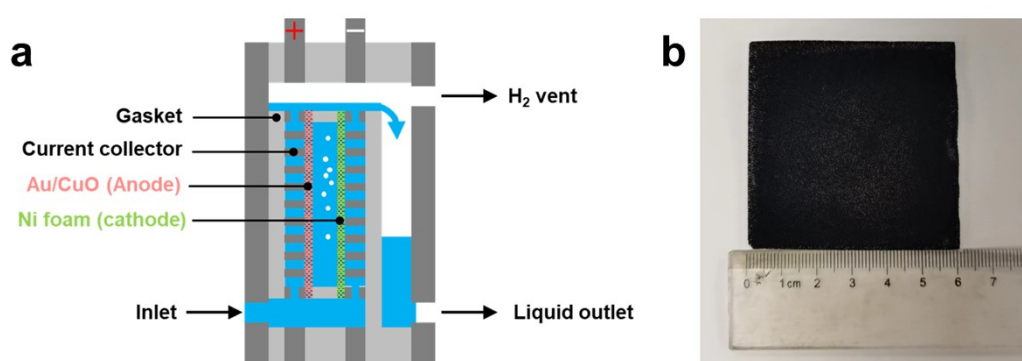


Figure S29. (a) Schematic illustration of the membrane-free flow electrolyzer. (b) Photographs of Au/CuO catalyst on Ni foam.

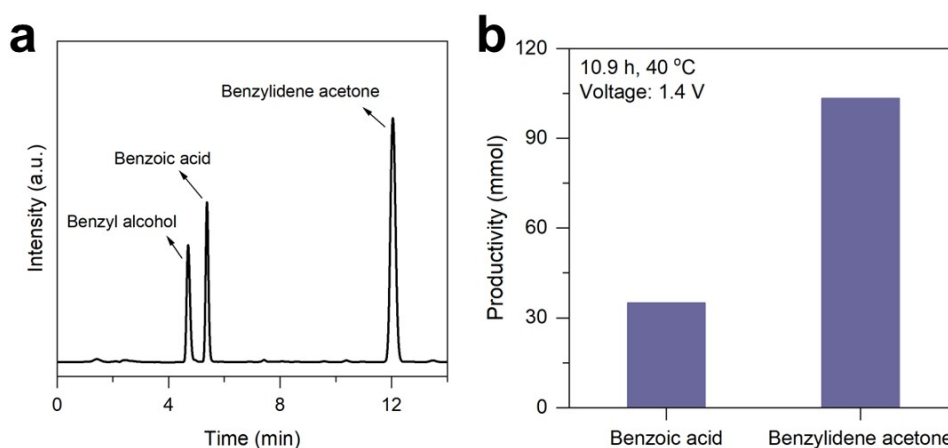


Figure S30. (a) HPLC chromatogram of benzyl alcohol oxidation products over Au/CuO catalyst using IP strategy at 1.4 V in 0.1 M KOH with 0.15 M benzyl alcohol and 0.3 M acetone at 40 °C in the stacked electrolyzer for 10.9 h. (b) Corresponding productivity of all products.



Figure S31. Model used for calculating the techno-economic analysis of sustainable benzylidene acetone electrosynthesis using benzyl alcohol as the feedstocks.

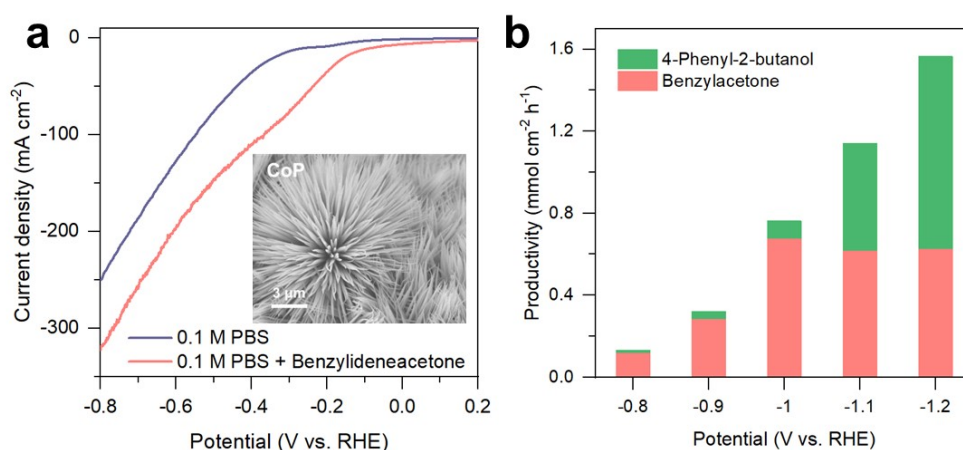


Figure S32. (a) LSV curves of CoP at scan rate of 10 mV s⁻¹ in 0.1 M PBS (pH = 7) with or without 50 mM benzylidene acetone. Inset shows the SEM image of CoP nanorods. (b) Cathodic products of benzylidene acetone reduction over CoP obtained at different potentials.

CoP nanorod array was prepared by phosphating of α -Co(OH)₂ precursor. The benzylidene acetone reduction reaction (denoted as BRR) was carried out in 0.1 M PBS (pH = 7) with 0.05 M benzylidene acetone. The LSV curves in Figure S32a show that the current density of BRR achieves 20 mA cm⁻² at potential of -0.15 V vs. RHE over CoP, which is more positive than HER (-0.34 V vs. RHE), demonstrating that BRR is kinetically more favorable than HER. CA measurements were then carried out to investigate the products of BRR over CoP at different potentials. As shown in Figure S32b, benzylacetone is the main product when the reaction potential is lower than -1.0 V vs. RHE with selectivity >89%, further increasing the potential causes over-reduction to produce 4-phenyl-2-butanol.

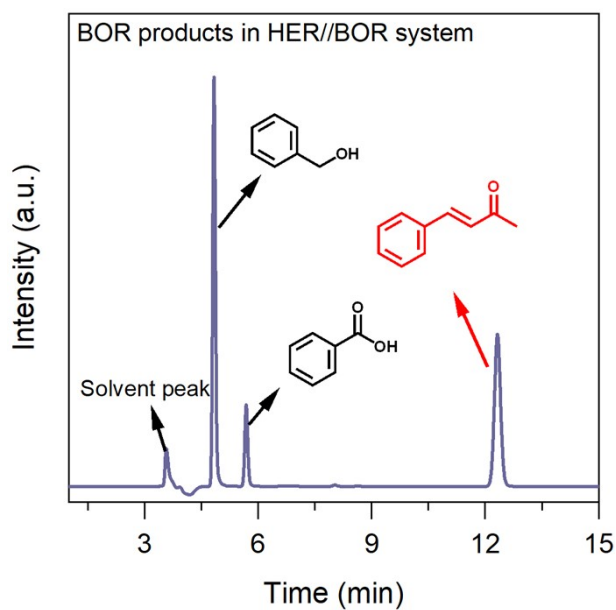


Figure S33. HPLC chromatogram of benzyl alcohol oxidation products over Au/CuO catalyst in HER//BOR system at 1.5 V.

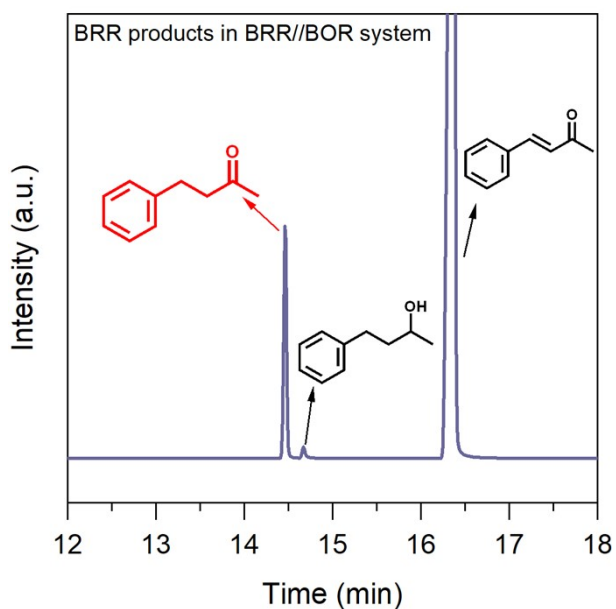


Figure S34. HPLC chromatogram of benzylidene acetone electroreduction products over CoP catalyst in BRR//BOR system at 1.5 V.

Supplementary Notes

Supplementary Note 1

Model construction. The model of bulk CuO was constructed with the space group $C2/c$, which lattice parameters are $a = 4.684 \text{ \AA}$, $b = 3.423 \text{ \AA}$, $c = 5.123 \text{ \AA}$, $\alpha = \gamma = 90^\circ$, and $\beta = 99.54^\circ$ according to the results of X-ray diffraction measurement data (Figure S2) and previous literature.⁶ The unit cell of CuO contained four Cu atoms and four O atoms. According to the image of CuO and Au/CuO (Figure S2), the exposed facet of CuO is (111) surface. The CuO (111) surface has been widely chosen as an ideal model system to investigate the structure, stability, adsorption properties, and reaction mechanism.^{7,8} Therefore, the (111) facet of CuO was cleaved, containing four layers of Cu atoms and four layers of O atoms. The supercell of CuO (111) was $4 \times 2 \times 1$ in the a -, b -, and c - directions. The vacuum thickness was set to be 20 \AA along the c -axis direction to minimize interlayer interactions. The model of the pristine CuO (111) surface was defined as CuO-P. Electron paramagnetic resonance (EPR) measurements indicated that both CuO and Au/CuO contain oxygen vacancies. The model of the CuO (111) surface with one O_{3c} oxygen vacancy was built and defined as CuO- O_{3C} , the chemical formula of which was $Cu_{64}O_{63}$. The model of the CuO (111) surface with one O_{4c} oxygen vacancy was built and defined as CuO- O_{4C} , the chemical formula of which was $Cu_{64}O_{63}$. The formation energies of two kinds of oxygen vacancies with various coordination numbers were then evaluated and compared theoretically; the model and results were displayed in Figure S24.

The model of bulk Au was constructed with the space group $Fm\bar{3}m$ according to the previous literature.⁹ The lattice parameters are $a = b = c = 4.072 \text{ \AA}$, $\alpha = \gamma = \beta = 90^\circ$. According to the experiment observation (Figures S2 and S3), the exposed surface of Au particles is the (111) surface. Thus, one Au_{20} cluster with the (111) surface exposed was constructed according to Li and Wang's work.¹⁰ This Au_{20} cluster has 1, 3, 6, and 10 atoms in four layers from top to bottom, respectively, with the atoms arranged according to the fcc stacking.

The Au_{10} cluster was constructed using the same method as the Au_{20} cluster, maintaining the high symmetry of the regular tetrahedron structure to reduce computational complexity.¹¹ This Au_{20} cluster has 1, 3, and 6 atoms in three layers from top to bottom, respectively, with the atoms arranged according to the fcc stacking. Then the model of Au/CuO was constructed

by putting one Au₁₀ cluster on the CuO-O_{3C} (111) surface with oxygen vacancy. The chemical formula of Au/CuO is Au₁₀Cu₆₄O₆₃.

In order to calculate the adsorption energy of benzyl alcohol and the Gibbs free energy landscapes of electrocatalytic oxidation from benzyl alcohol to benzaldehyde over Au, CuO-O_{3C}, and Au/CuO, a series of reaction intermediates, Ph-CH₂OH*, Ph-CH₂OH* + OH*, Ph-CH₂O*, Ph-CH₂O* + OH*, and Ph-CHO* (* is the reaction site over Au, CuO-O_{3C}, or Au/CuO) were constructed by putting corresponding molecules at the reaction sites.

Computational methods. It is proposed that the oxidation reaction from benzyl alcohol to benzylidene acetone with acetone involved two phases. At the interface between the solution and the heterogeneous catalyst, benzyl alcohol is first converted to benzaldehyde under the electric field. The second stage is a homogeneous reaction process in solution where benzaldehyde and acetone react to form benzylidene acetone.

For the first stage, the spin-polarized density functional theory (DFT) calculations were performed through the Cambridge Sequential Total-Energy Package (CASTEP)¹² using a plane wave implementation at the generalized gradient approximation (GGA) Perdew-Burke-Ernzerhof (PBE)¹³ level. The ionic cores were described by the ultrasoft pseudopotentials¹⁴ to improve transferability and reduce the number of plane waves needed in the expansion of the Kohn-Sham orbitals. The Broyden-Fletcher-Goldfarb-Shanno (BFGS) algorithm was employed to search the potential energy surface during optimization.¹⁵ The cutoff energy was set as 400 eV referred to our previous work. The geometry optimization was based on the following points: (i) an energy tolerance of 1×10^{-5} eV/atom, (ii) a maximum force tolerance of 0.03 eV/Å, and (iii) a maximum displacement tolerance of 1×10^{-3} Å. The Tkatchenko-Scheffler (TS) method was implemented to correct the van der Waals interactions.¹⁶ The Brillouin zone was sampled using the Monkhorst-Pack scheme with a $3 \times 3 \times 1$ *k*-point mesh for the CuO-O_{3C} (111) and Au/CuO (111) surface. For the Au₂₀ cluster and isolated molecule, a $1 \times 1 \times 1$ *k*-point mesh was used.¹⁷ The frequency was obtained by calculating the phonon density of states using the finite displacement method. The Gibbs free energies of reactant, intermediate, and product were obtained with eq 1 through analyzing their frequency:

$$G = E + ZPE + kT \int F(\omega) \ln [1 - \exp(-\frac{\hbar\omega}{kT})] d\omega \quad (1)$$

where E was the total energy, ZPE was the zero-point energy which could be directly read

from the output, the term $kT \int F(\omega) \ln [1 - \exp(-\frac{\hbar\omega}{kT})] d\omega$ was the correction of Gibbs free energy which could also be read from the output.

For the second stage, the spin-polarized density functional theory (DFT) calculations were performed using the Gaussian package of programs.¹⁸ Geometry optimizations and frequency calculations were calculated at the DFT B3LYP/6-311G(d,p) level.¹⁹ The Grimme's dispersion correction with Becke-Johnson damping (GD3BJ) were included.²⁰ Implicit solvent model Solvation Model Based on Density (SMD) was applied to simulate solvent effects.²¹ The single-point energy was calculated at B3LYP/def2TZVP level. The Gibbs free energy (G) of molecule was obtained by the following equation:

$$G_M = E_{correct} + E_{sp} \quad (2)$$

where $E_{correct}$ was the thermal correction to G from frequency calculations, E_{sp} was the single point energy.

The formation energies of oxygen vacancy were calculated as:

$$E_{form} = E_{O_{vac}} + 0.5 * E_{O_2} - E_p \quad (3)$$

where $E_{O_{vac}}$ is the total energy of the CuO (111) surface with one oxygen vacancy, E_{O_2} is the total energy of O₂, and E_p is the total energy of the CuO-P surface.

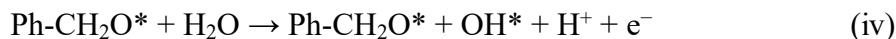
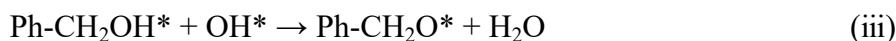
The adsorption energy (E_{ads}) of benzyl alcohol was calculated with Eq. 4:

$$E_{ads} = E_{Ph-CH_2OH^*} - E_{Ph-CH_2OH} - E_* \quad (4)$$

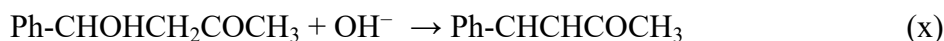
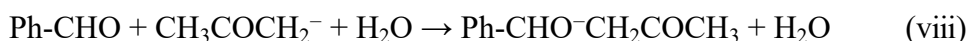
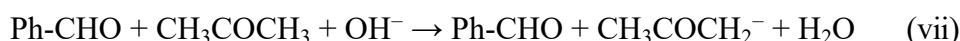
where $E_{Ph-CH_2OH^*}$, E_{Ph-CH_2OH} , and E_* are the energies of Ph-CH₂OH*, Ph-CH₂OH, and *, respectively.

The electrocatalytic oxidation of benzyl alcohol to benzaldehyde over Au or Au/CuO occurs in six consecutive steps (i-vi):





The aldol condensation reaction between benzaldehyde and ketones contains four steps (vii-x):

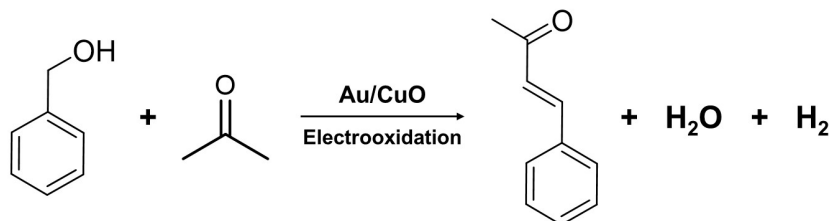


The elementary reaction step of the oxygenation of benzyl alcohol to benzylidene acetone was listed in Table xx. The Gibbs free energy change (ΔG) of each elementary step was calculated as the difference between the G of the product and that of the reactant. The computational hydrogen electrode approximation ($0.5\text{H}_2 \rightarrow \text{H}^+ + \text{e}^-$, $\text{pH} = 0$, $p = 1 \text{ atm}$, $T = 298.15 \text{ K}$) was used to deal with the G of proton and electron²².

Supplementary Note 2

Green chemistry metrics^{23,24}

(1) Atom Economy (AE)



For a given reaction, AE is defined as the ratio of the molecular weight of the desired product to the total molecular weight of all reagents, as determined by the stoichiometric equation. For electrochemical synthesis of benzylidene acetone, AE was calculated to be 89.0%, as shown below.

$$\text{AE} = \frac{\text{MW of desired product}}{\text{MW of reagents}} = \frac{146.19}{106.12 + 58.08}$$

(2) Environmental factor (E-factor)

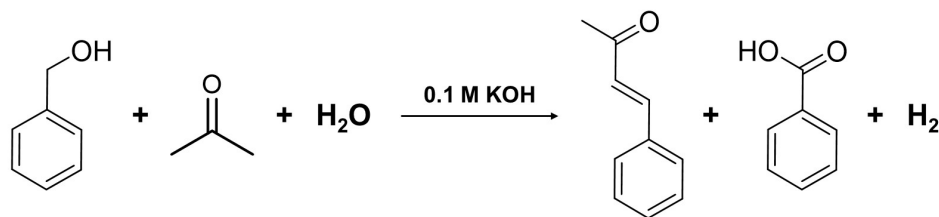


Table S1 Calculation of environmental factor in electrochemical synthesis of benzylidene acetone.^{a, b}

Raw materials and byproducts	Quantity (kg per kg of benzylidene acetone)
benzyl alcohol	0.88 (complete reaction)
acetone	0.80 (residue of 0.46)
KOH (80% recycle)	0.092
benzoic acid	0.16
water	81.48
E-Factor	0.71

[a] H₂ is also considered a desirable product and is therefore not included in the waste for E-factor calculation. Additionally, water used in the process was excluded from the E-factor calculation.

[b] The data was based on the results shown in Figure 2c.

E-factor is defined as the mass ratio of waste to the desired product (the equation is shown below).

$$\text{E - factor} = \frac{\text{Mass of wastes}}{\text{Mass of desired product}}$$

The E-factor is used to evaluate the environmental impact of a production process, with a lower E-factor being more desirable. The ideal E-factor is zero. For the electrochemical synthesis of benzylidene acetone, we first compiled the amounts of raw materials and byproducts per kilogram of benzylidene acetone (Table S1, based on the catalytic results in Figure 2c) and then calculated the corresponding E-factor. Since H₂ is also a desirable product, it was excluded from the waste calculation. As a result, the E-factor for the electrochemical synthesis of benzylidene acetone was determined to be 0.71, indicating that the method is

environmentally friendly.

(3) Carbon efficiency (CE)

Table S2 Calculation of carbon efficiency in electrochemical synthesis of benzylidene acetone.^a

Carbonaceous chemicals	Mass of carbon (kg)
benzyl alcohol	0.78
acetone	0.66
benzylidene acetone	0.93
benzoic acid	0.14

[a] The data was based on the results shown in Figure 2c.

CE is defined as the ratio of the carbon mass in the final product to the total carbon mass in the reactants, as expressed in the equation below.

$$CE = \frac{\text{Mass of carbon in the product}}{\text{Total mass of carbon in the reactants}}$$

Table S2 presents the carbonaceous chemicals involved in the electrochemical synthesis of benzylidene acetone along with their corresponding carbon mass. The data is derived from the catalytic results shown in Figure 2c. Based on these values, the CE for the electrochemical synthesis of benzylidene acetone was determined to be 74%. Note that acetone is used in excess; however, the remaining acetone can be recovered and reused for future reactions.

Supplementary Note 3

TEA analysis. To evaluate the economic feasibility of producing sustainable benzylidene acetone via electrosynthesis using benzyl alcohol and acetone as feedstocks, we performed a techno-economic analysis (TEA) utilizing a modified model introduced by Sargent et al.²⁵⁻²⁷

Figure S31 outlines the components used to compute both the total basic manufacturing costs and product profits. This methodology divides prices into two main segments: manufacturing costs and profits. Manufacturing costs encompass feedstock expenses, catalyst expenditures, separation device outlays, electricity charges, separation costs, and operational expenses. Profits, on the other hand, consist of hydrogen dividends and benzylidene acetone dividends.

In this study, we conducted a TEA calculation presuming optimized conditions for the flow cell operation. Hereafter, we provide an exhaustive compilation of the fundamental assumptions:

Here, we carry out a TEA calculation for the case where the optimized condition of the flow cell is performed. Below is a full list of the assumptions made:

1. Catalyst costs are composed of two parts: Au/CuO, and Ni Foam. We assume a 1 m² area of the catalyst is used for electrolysis with a lifetime of 10 years. Separation device costs are assumed to be 10 % of the catalyst cost. The market prices of Au and CuO are 70000 kg⁻¹ and 3 \$ kg⁻¹, respectively. The market prices of Ni foam are 18 \$ m⁻².
2. Electricity cost is assumed as 0.03 \$ kW h⁻¹ based on recently reported work.
3. Separation costs include the products separation (benzyl alcohol, acetone and benzylidene acetone). The total separation costs are assumed to be 30 % of the electricity cost.
4. Feedstock cost includes the benzyl alcohol and acetone. The price of benzyl alcohol is 2000 \$ t⁻¹ and acetone is 990 \$ t⁻¹ separately.
5. Operation costs are assumed as 10 % of catalyst costs and separation device costs.
6. The operational time of electrolysis is assumed to be 80 % of a day (19.2 h).
7. The selectivity rate of the benzyl alcohol convert to benzylidene acetone is assumed 75 %. Thus, electrolysis will convert 98.75 tons of benzyl alcohol and 53.04 tons of acetone to 100 tons of benzylidene acetone per day.
8. The prices of benzylidene acetone and hydrogen are assumed as 3500 \$ t⁻¹ and 1900 \$ t⁻¹.

Calculations details

The total basic manufacture costs

(1) Feedstock costs

Feedstock costs per ton = (Cost of benzyl alcohol × Mass of benzyl alcohol reacted) + (Cost of acetone × Mass of acetone reacted) / Mass of benzylidene acetone produced per day

$$[(2000 \times 98.75) + (990 \times 53.04)] / 100\$ = 2500.09 \$$$

(2) Electricity costs

We calculate the total charge needed to produce 100 tons of benzylidene acetone per day, which represents the reaction of benzyl alcohol convert to benzaldehyde.

$$Q = (\text{Mass of benzyl alcohol consumed} / \text{Molar mass of benzyl alcohol} \times N \times F) / \text{Faradaic efficiency} / (1 - 20 \%)$$

Where Q is the total charge, F is the Faraday constant (96485 C), N is 2 since benzyl alcohol to benzaldehyde is a two-electron reaction process.

$$[(100 \times 10^6) / 108.14 \times 2 \times 96485 / 0.60 / (1 - 20 \%)] \text{ C} = 3.72 \times 10^{11} \text{ C}$$

The corresponding current:

$$I = Q / t$$

$$[3.72 \times 10^{11} / (19.2 \times 3600)] \text{ A} = 5378466.4 \text{ A}$$

The corresponding power:

$$\text{Energy consumption per day} = U I t$$

$$(1.4 \times 5378466.4) / 1000 \times 19.2 \text{ kW h} = 144573.18 \text{ kW h}$$

Thus, the electricity cost per ton for benzylidene acetone generation:

$$\text{Electricity costs per ton} = (\text{Energy consumption per day} \times \text{Cost per kW h}) / \text{Mass of benzylidene acetone per day}$$

$$[(144573.18 \times 0.03) / 100] \$ = 43.37 \$$$

(3) The total separation costs

$$\text{The total separation costs per ton} = \text{Electricity cost per ton} \times 30 \%$$

$$(43.37 \times 30 \%) \$ = 13.01 \$$$

(4) Catalyst costs and Separation device costs

Catalyst costs per square meter according the ICP result. The loading mass of Au and CuO per square meter of Ni Foam is 1.8 g and 5.4 g.

$$\text{Au price (m}^2\text{)} = \text{The mass of Au} \times \text{The price of Au}$$

$$1.8 \times 70 \$ = 126.0 \$$$

$$\text{CuO price (m}^2\text{)} = \text{The mass of CuO} \times \text{The price of CuO}$$

$$5.4 \times 0.003 \$ = 0.02 \$$$

The price of Ni Foam is \$ 18.00 per square meter.

$$\text{Catalyst costs (m}^2\text{)} = \text{Au price (m}^2\text{)} + \text{CuO price (m}^2\text{)} + \text{Ni Foam price (m}^2\text{)}$$

$$(126.0 + 0.02 + 18.0) \$ = 144.2 \$.$$

We evaluate the catalyst area needed. Based on the applied potential (1.4 V) and operating current density (33.0 mA cm⁻²), we can calculate the area of catalyst costs needed.

The area of catalyst costs needed = the current per day / the operating current density

$$[5378466.4 / (33 \times 10)] \text{ m}^2 = 16298.38 \text{ m}^2$$

Catalyst costs = The area of catalyst costs needed × Catalyst costs per square meter

$$(16298.38 \times 144.2) \$ = 2350226.83 \$$$

Separation device costs = Catalyst costs × 10 %

$$(2350226.83 \times 10 \%) \$ = 235022.68 \$$$

The costs for Catalyst and Separation device per ton = (Catalyst costs + Separation device cost) / (lifetime of electrolyzer / Mass of benzylidene acetone produced per day)

$$[(2350226.83 + 235022.68) / (10 \times 365) / 100] \$ = 7.08 \$$$

(5) Operation costs

Operation costs per ton = The costs for Catalyst and Separation devices per ton × 10 %

$$(7.08 \times 10 \%) \$ = 0.71 \$$$

The costs for manufacture

The costs for manufacture per ton = Feedstock costs per ton + Electricity cost per ton + The total separation costs per ton + The costs for Catalyst and Separation device per ton + Operation cost per ton

$$(2500.09 + 43.37 + 13.01 + 7.08 + 0.71) \$ = 2564.26 \$$$

The special dividends

Hydrogen is generated at the cathode and assumed as 100 % Faradaic efficiency.

Mass of hydrogen produced per day = $Q \times FE_{\text{Hydrogen}} / F / N \times \text{Molar mass of hydrogen}$

$$[(3.72 \times 10^{11} \times 100 \% / 96485 / 2 \times 2) \times 10^{-6}] \text{ t} = 3.85 \text{ t}$$

Profit of hydrogen per day = Mass of hydrogen produced per day × Market price

$$(3.85 \times 1900) \$ = 7325.5 \$$$

Profit of hydrogen per ton of benzylidene acetone = Profit of hydrogen per day / Mass of benzylidene acetone produced per day

$$(7325.5 / 100) \$ = 73.25 \$$$

The total profit

The profit per ton from this electrosynthesis can be calculated based on the market price of hydrogen in the cathode and benzylidene acetone in the anode.

The profit = The market price of benzylidene acetone + The market price of hydrogen – The costs for manufacture

$$(3500 + 73.25 - 2564.26) \$ = 1008.99 \$$$

Supplementary References

1. Z. Li, M. Shao, H. An, Z. Wang, S. Xu, M. Wei, D. Evans, X. Duan, *Chem. Sci.* **2015**, *6*, 6624–6631.
2. Z. Wei, H. Wang, C. Zhang, K. Xu, X. Lu, T. Lu, *Angew. Chem. Int. Ed.* **2021**, *133*, 16758–16763.
3. C. McCrory, S. Jung, J. Peters, T. Jaramillo, *J. Am. Chem. Soc.* **2013**, *135*, 16977–16987.
4. G. Liu, M. Wang, Y. Wu, N. Li, F. Zhao, Q. Zhao, J. Li, *Appl. Catal. B* **2020**, *260*, 118199.
5. Y. Zhang, S. Chen, Y. Zhang, R. Li, B. Zhao, T. Peng, *Adv. Mater.* **2023**, *35*, 2210727.
6. A. Garcia, M. Kolb, C. Sanchez, J. Vos, Y. Birdja, Y. Kwon, G. Tremiliosi-Filho, M. Koper, *ACS Catal.* **2016**, *6*, 4491–4500.
7. Y. Guo, R. Hu, X. Zhou, J. Yu, L. Wang, *Appl. Surf. Sci.* **2019**, *479*, 989–996.
8. P. Zhou, X. Lv, S. Tao, J. Wu, H. Wang, X. Wei, T. Wang, B. Zhou, Y. Lu, T. Frauenheim, X. Fu, S. Wang, Y. Zou, *Adv. Mater.* **2022**, *34*, 2204089.
9. I. Suh, H. Ohta, Y. Waseda, *J. Mater. Sci.* **1988**, *23*, 757–760.
10. J. Li, X. Li, H. Zhai, L. Wang, *Science* **2003**, *299*, 864–867.
11. Z. Li, C. Ciobanu, J. Hu, J. Palomares-Baez, J. Rodríguez-López, R. Richards, *Phys. Chem. Chem. Phys.* **2011**, *13*, 2582.
12. S. Clark, M. Segall, C. Pickard, P. Hasnip, M. Probert, K. Refson, M. Payne, *Z Kristallogr Cryst Mater* **2005**, *220*, 567–570.
13. J. Perdew, K. Burke, M. Ernzerhof, *Phys. Rev. Lett.* **1996**, *77*, 3865–3868.
14. D. Vanderbilt, *Phys. Rev. B* **1990**, *41*, 7892–7895.
15. J. Head, M. Zerner, *Chem. Phys. Lett.* **1985**, *122*, 264–270.
16. A. Tkatchenko, M. Scheffler, *Phys. Rev. Lett.* **2009**, *102*, 073005.
17. H. Monkhorst, J. Pack, *Phys. Rev. B* **1976**, *13*, 5188–5192.
18. M. Frisch, G. Trucks, H. Schlegel, et al, *Gaussian Inc. Wallingford CT*, **2016**, *1*, 572.
19. P. Stephens, F. Devlin, C. Ashvar, C. Chabalowski, M. Frisch, *Faraday Discuss.* **1994**, *99*,

103.

20. S. Grimme, J. Antony, S. Ehrlich, H. Krieg, *J. Chem. Phys.* **2010**, *132*, 154104.
21. A. Marenich, C. Cramer, D. Truhlar, *J. Phys. Chem. B* **2009**, *113*, 6378–6396.
22. Á. Valdés, Z. Qu, G. Kroes, J. Rossmeisl, J. Nørskov, *J. Phys. Chem. C* **2008**, *11*, 9872–9879.
23. Roger A. Sheldon, *Chem. Soc. Rev.* **2014**, *41*, 1437-1451.
24. Roger A. Sheldon, *Chem. Commun.* **2008**, *29*, 3352-3365.
25. W. Leow, Y. Lum, A. Ozden, Y. Wang, D. Nam, B. Chen, J. Wicks, T. Zhuang, F. Li, D. Sinton, E. Sargent, *Science* **2020**, *368*, 1228–1233.
26. Y. Lum, J. Huang, Z. Wang, M. Luo, D. Nam, W. Leow, B. Chen, J. Wicks, Y. Li, Y. Wang, C. Dinh, J. Li, T. Zhuang, F. Li, T. Sham, D. Sinton, E. Sargent, *Nat. Catal.* **2020**, *3*, 14–22.
27. N. Meng, J. Shao, H. Li, Y. Wang, X. Fu, C. Liu, Y. Yu, B. Zhang, *Nat. Commun.* **2022**, *13*, 5452.